Supplementary Information

Multiscale Charge-Carrier Dynamics Governed by Surface Energetics in Facet-Engineered $NaNbO_3/FeVO_4$ Photoanodes

Nitika Garg,[a] Pabitra Kumar Nayak,[a] Ambika Prasad Kar,[a] Sandeep Kumar,[a,c] Dibyajyoti Ghosh,[a,b] Pramit K. Chowdhury,[a] and Ashok K. Ganguli[a,d*]

[a] Department of Chemistry, Indian Institute of Technology Delhi, New Delhi 110016, India
[b] Department of Materials Science and Engineering, Indian Institute of Technology Delhi, New Delhi 110016, India
[c] Department of Chemistry, Motilal Nehru College, University of Delhi, Benito Juarez Marg, South Campus, New Delhi 110021, India
[d] Department of Chemical Sciences, Indian Institute of Science Education and Research Berhampur, Ganjam, Odisha-760003, India

[*] Corresponding author e-mail: *ashok@chemistry.iitd.ac.in*

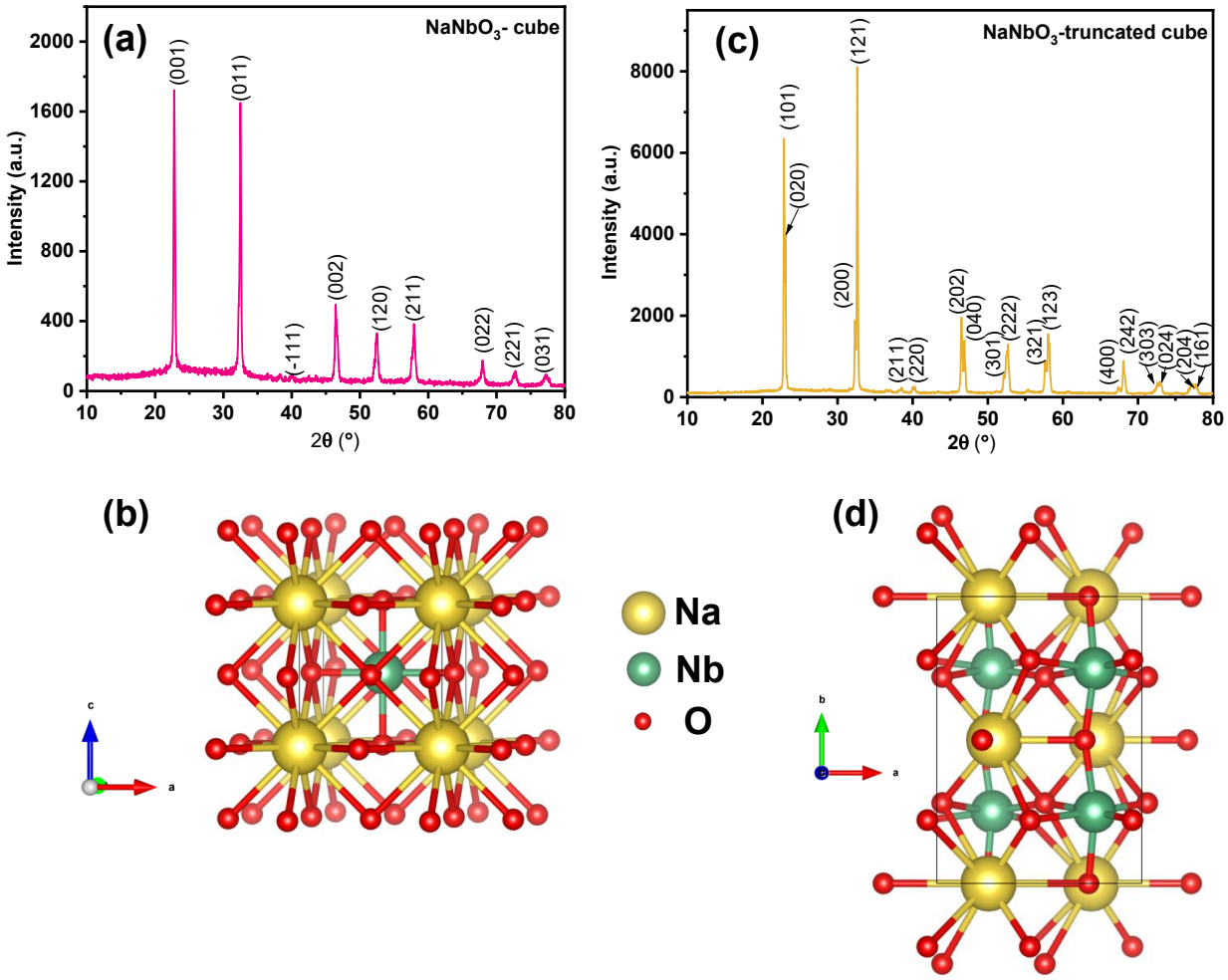

Figure S1: Indexed PXRD pattern of **(a)** $NaNbO_3$-1 (cube) and **(c)** $NaNbO_3$-2 (truncated cube). The corresponding crystal structure for **(b)** $NaNbO_3$-1 (cube) and **(d)** $NaNbO_3$-2 (truncated cube).

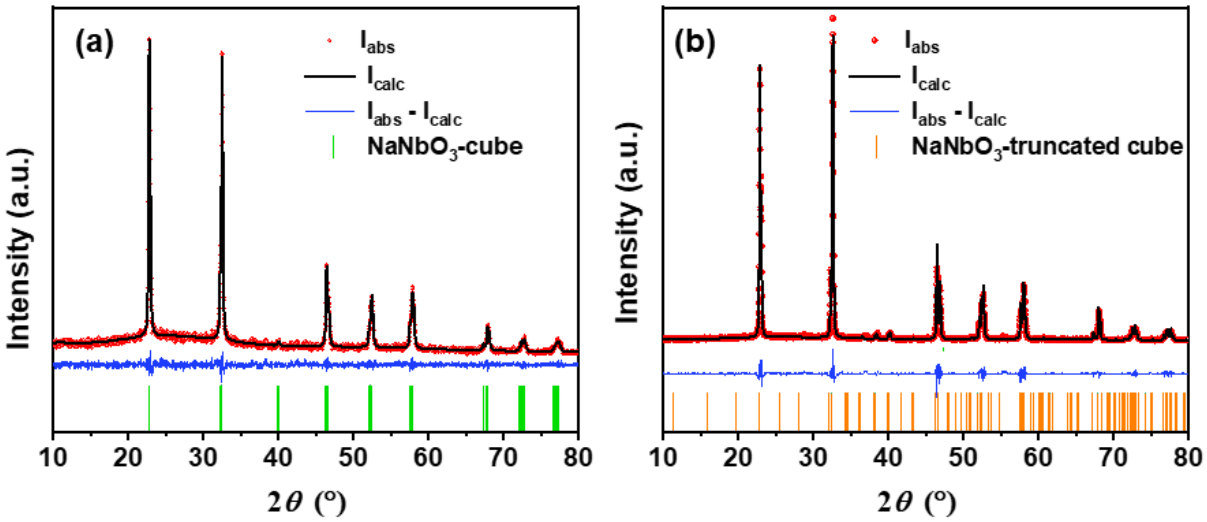

Figure S2: Rietveld refined powder x-ray pattern of **(a)** $NaNbO_3$-cube and **(b)** $NaNbO_3$-truncated cube.

‘

Table S1: Crystallographic details of $NaNbO_3$-1 (cube) and $NaNbO_3$-2 (truncated cube) from Rietveld refinement.

Parameter	**$NaNbO_3$-1 (cube)**	**$NaNbO_3$-2 (truncated cube)**
Space group	P2/m	$P2_1ma$
Space group number	10	26
a (Å)	3.9187(3)	5.5148(1)
b (Å)	3.8932(2)	7.7777(1)
c (Å)	3.9119(3)	5.5698(4)
α (°)	90.000	90.000
β (°)	89.487(7)	90.000
γ (°)	90.000	90.000

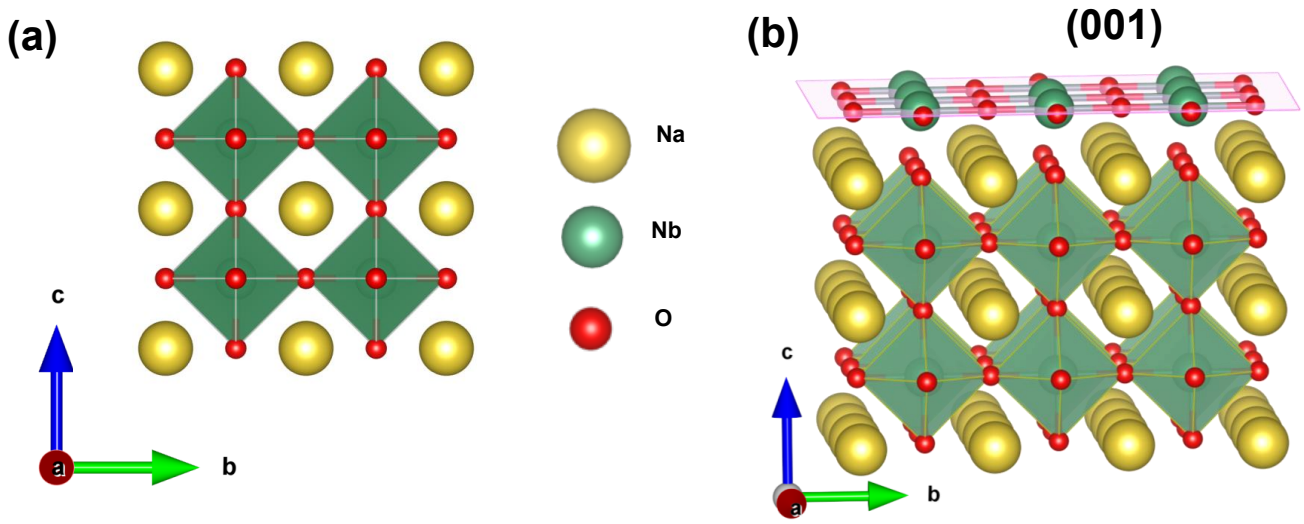

Figure S3: **(a)** Crystal structure of $NaNbO_3$-1 (cube) and **(b)** corresponding (001) exposed plane in monoclinic crystal system of $NaNbO_3$-1 (cube).

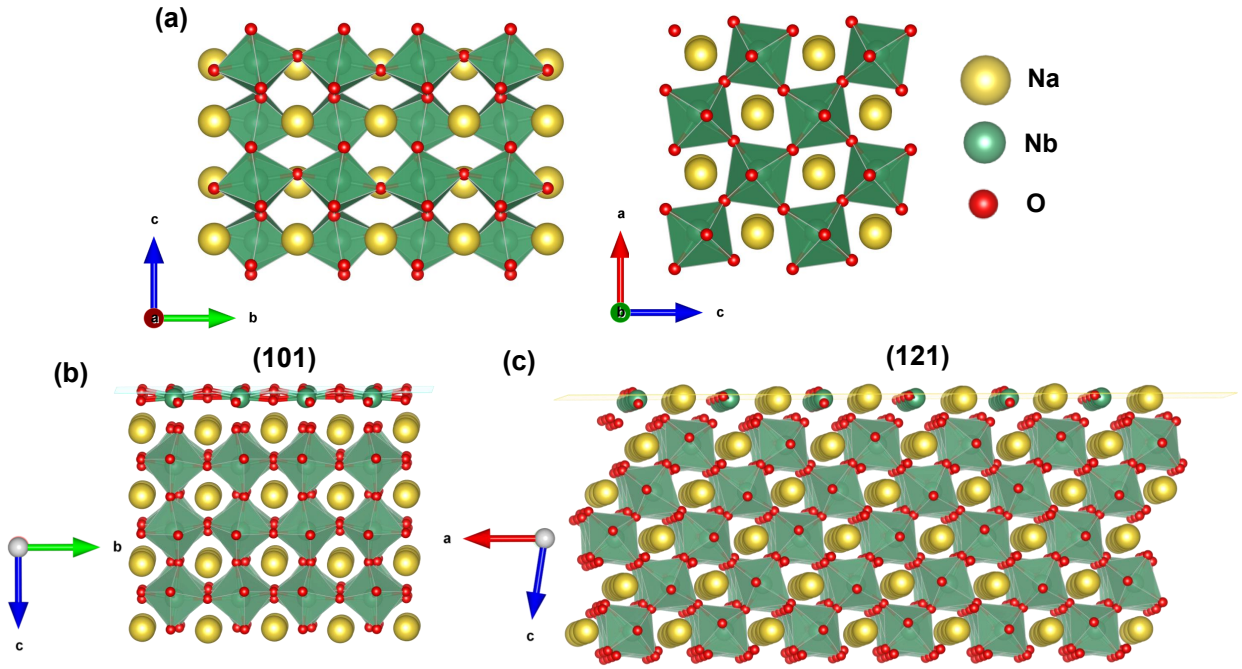

Figure S4: **(a)** Crystal structure of $NaNbO_3$-2 (truncated cube), corresponding exposed planes **(b)** (101) and **(c)** (121) in orthorhombic crystal system of $NaNbO_3$-2 (truncated cube).

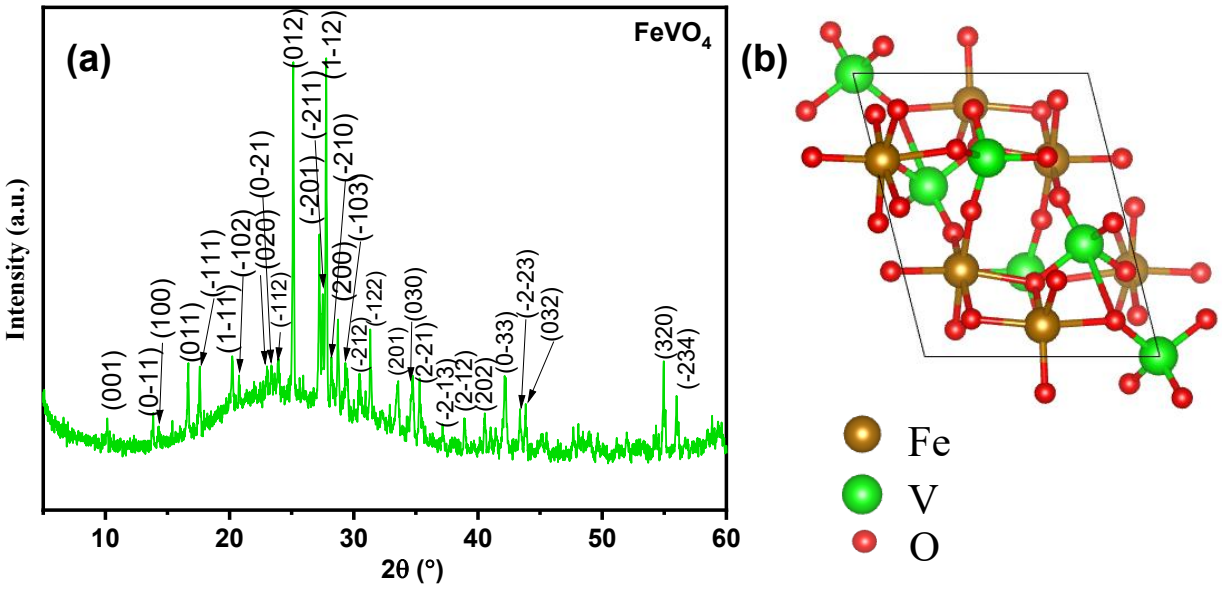

Figure S5: **(a)** Indexed PXRD pattern and **(b)** the corresponding crystal structure of $FeVO_4$.

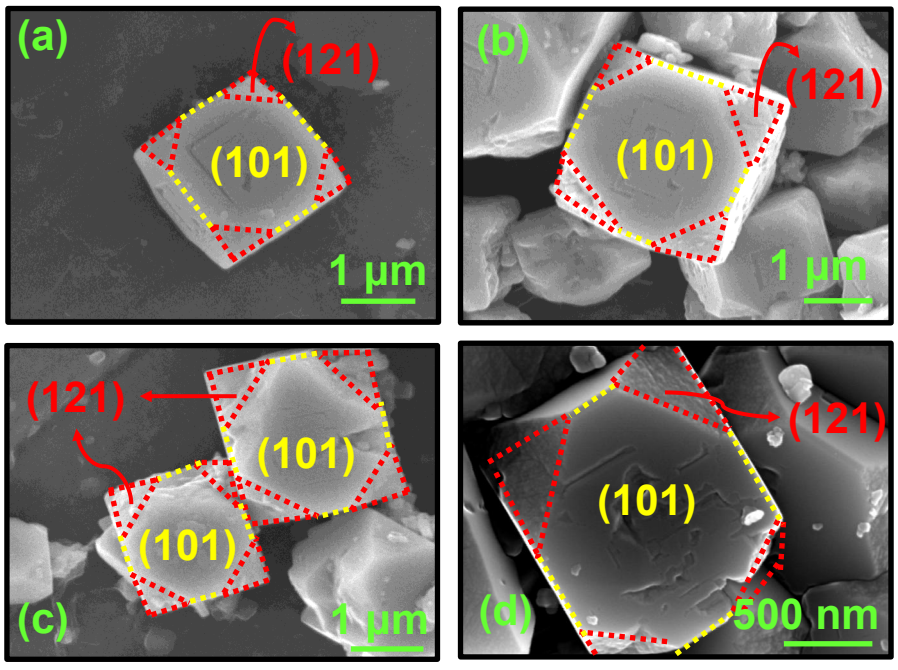

Figure S6: FESEM images of $NaNbO_3$-truncated cube recorded at different magnifications. **(a)-(d)** show the characteristic truncated-cube morphology, where the facets have been labelled, highlighting the coexistence of multiple exposed crystallographic facets.

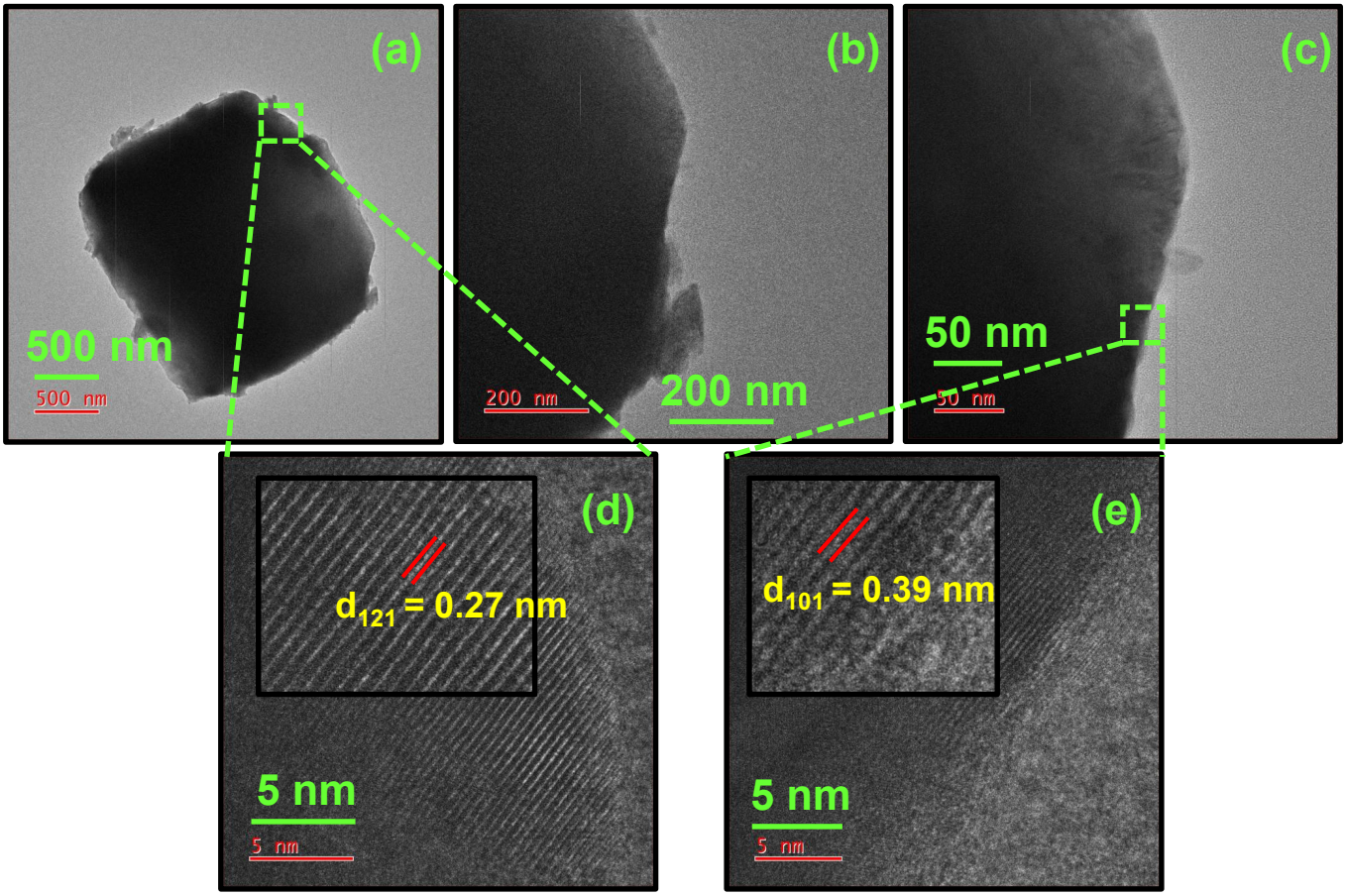

Figure S7: TEM and HRTEM images of $NaNbO_3$-truncated cube at different magnifications. **(a-c)** show the particle morphology and the regions selected for lattice analysis, while **(d)** and **(e)** present the corresponding magnified HRTEM images with measured lattice spacings of 0.27 nm and 0.39 nm, indexed to the (121) and (101) planes, respectively.

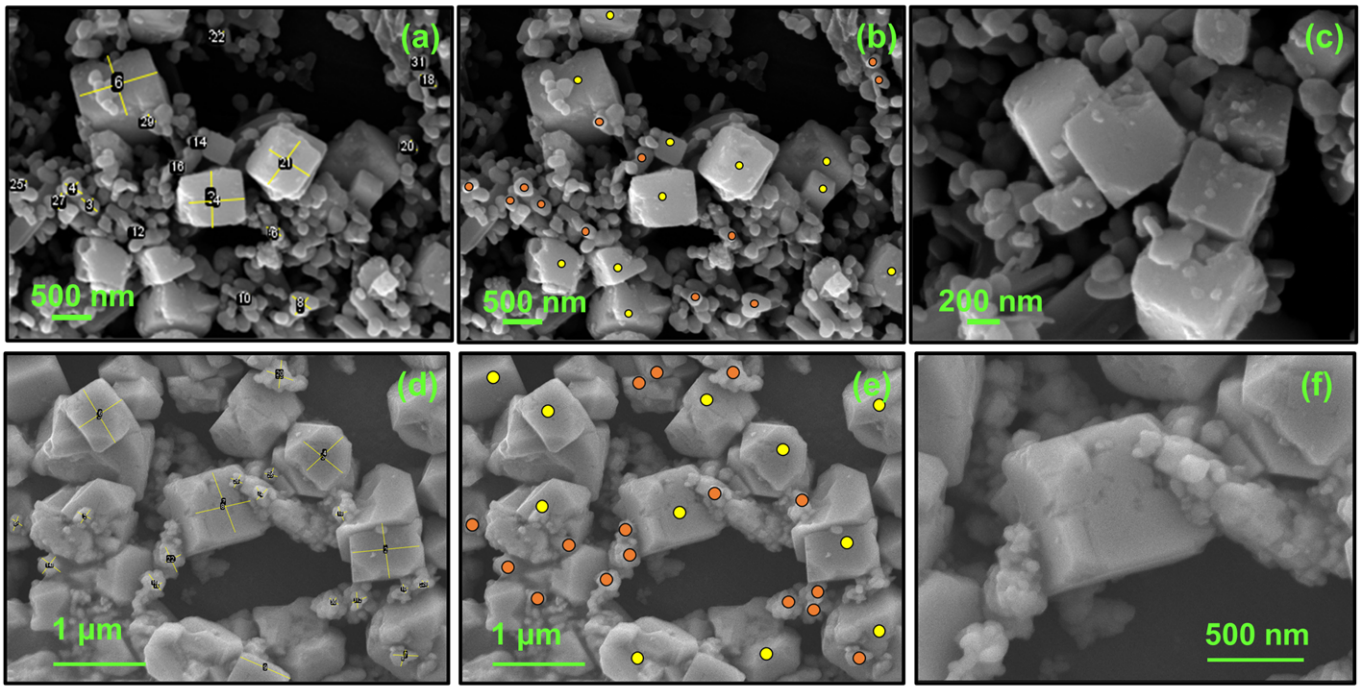

Figure S8: Representative SEM micrographs used for the semi-quantitative population analysis of particle morphologies in the $NaNbO_3/FeVO_4$ heterostructures. **(a-c)** $NaNbO_3$-cube/$FeVO_4$ sample and **(d-f)** $NaNbO_3$-truncated cube/$FeVO_4$ sample at different magnifications. **(a)** and **(d)** show the identification and size measurement of faceted plate-like crystals, while panels **(b)** and **(e)** illustrate the particle counting used for population estimation, where yellow and orange markers indicate faceted plates and irregular particles, respectively.

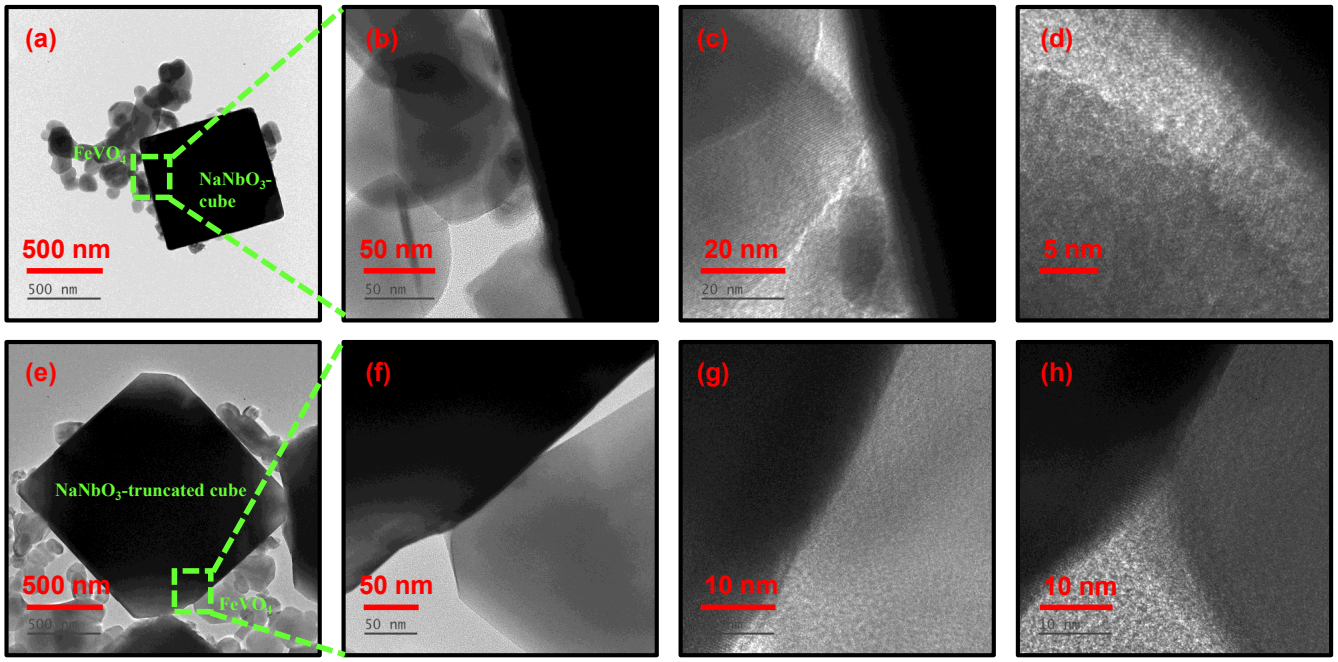

Figure S9: HRTEM micrographs of **(a-d)** $NaNbO_3$-cube/$FeVO_4$, **(e-h)** $NaNbO_3$-truncated cube/$FeVO_4$ at different magnifications.

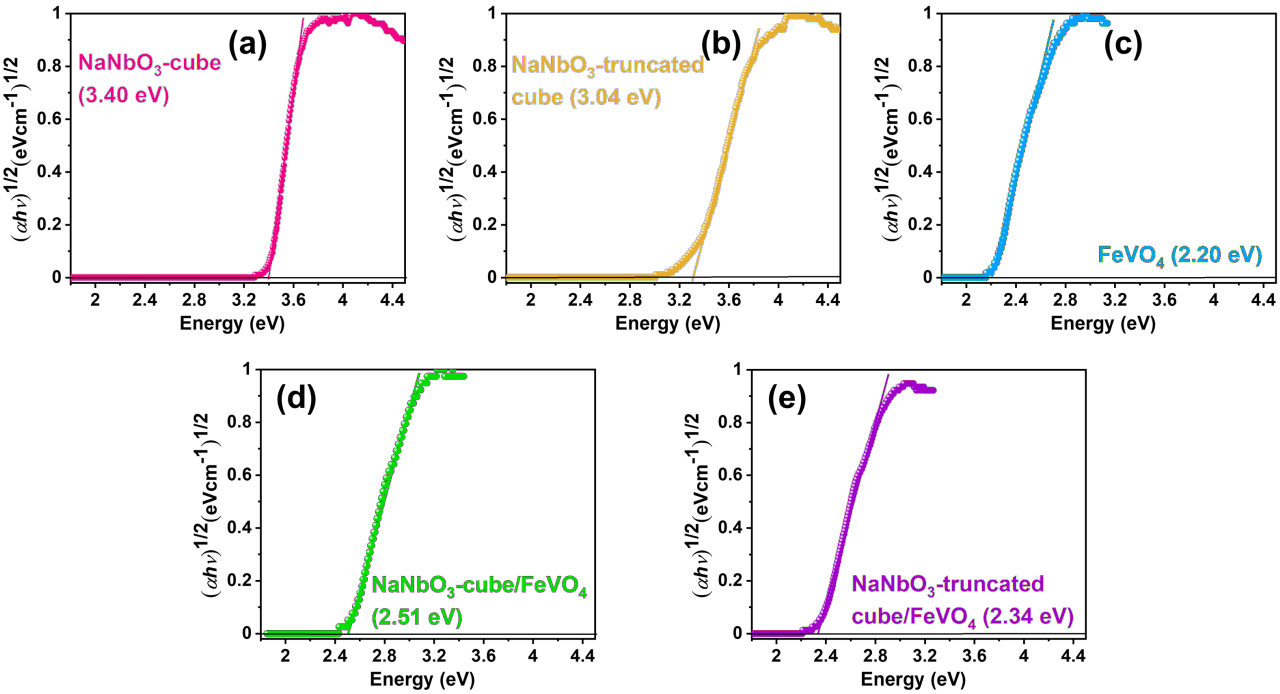

Figure S10: Tauc plots for **(a)** $NaNbO_3$-cube, **(b)** $NaNbO_3$-truncated cube, **(c)** $FeVO_4$, **(d)** $NaNbO_3$-cube/$FeVO_4$, and **(e)** $NaNbO_3$-truncated cube/$FeVO_4$, showing estimated band gap energies of 3.40, 3.04, 2.20, 2.51, and 2.34 eV, respectively.

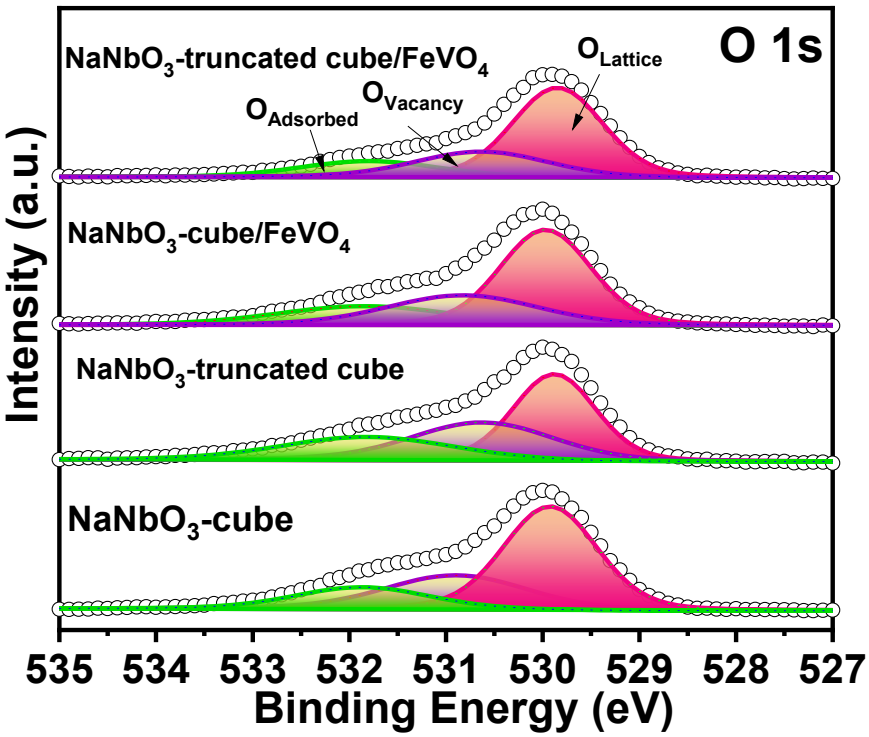

Figure S11: XPS deconvoluted spectra of O 1s in the synthesized photoelectrocatalysts.

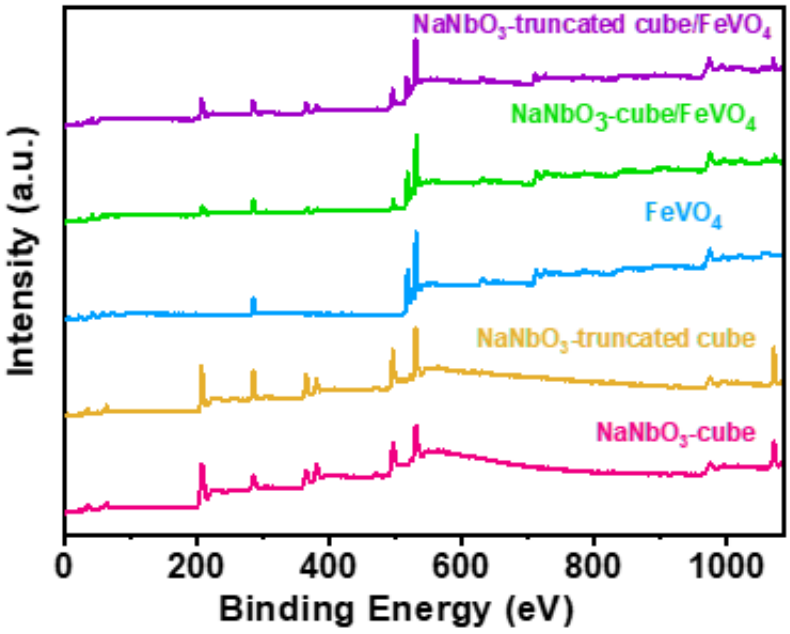

Figure S12: XPS survey spectra of the synthesized samples.

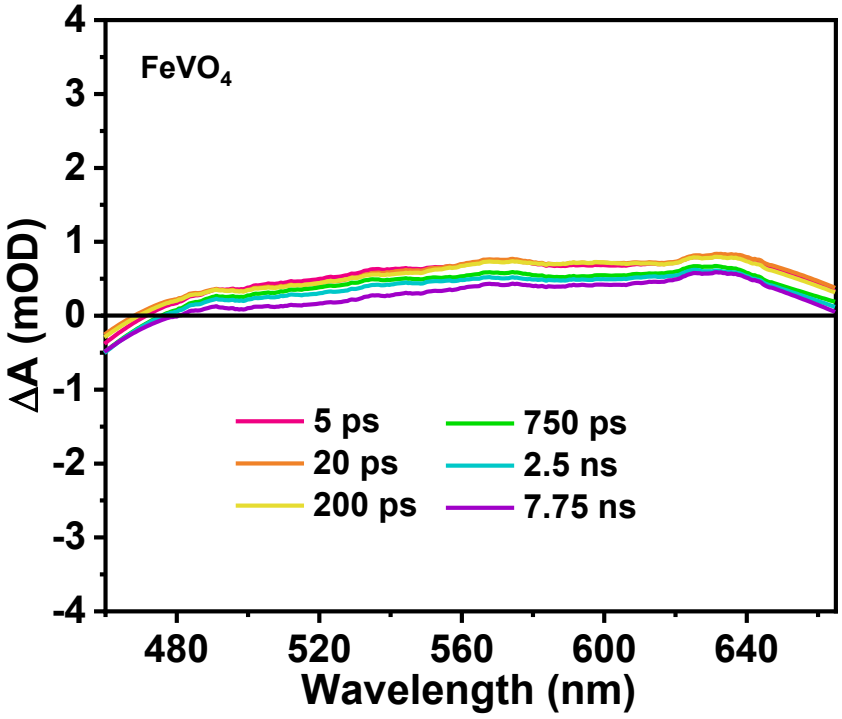

Figure S13: Ultrafast transient absorption spectra of $FeVO_4$ at different time delays after the 350 nm laser pump excitation.

Table S2: Ultrafast transient absorption spectroscopy fitted lifetime components and their relative contributions for the synthesized samples.

S. No.	**Material**	τ_1 (ps)	τ_2 (ps)	τ_3 (ps)	τ_4 (ps)
1	$NaNbO_3$-cube	0.369 (72.1%)	—	394 (12%)	>8000 (15.9%)
2	$NaNbO_3$-truncated cube	0.379 (60.6%)	122 (9.6%)	1300 (13%)	>8000 (16.8%)
3	$NaNbO_3$-cube/$FeVO_4$	0.414 (57.2%)	94 (7.1%)	2840 (18.8%)	>8000 (16.8%)
4	$NaNbO_3$-truncated cube/$FeVO_4$	0.575 (45%)	41.1 (8.4%)	5630 (14%)	>8000 (32.6%)

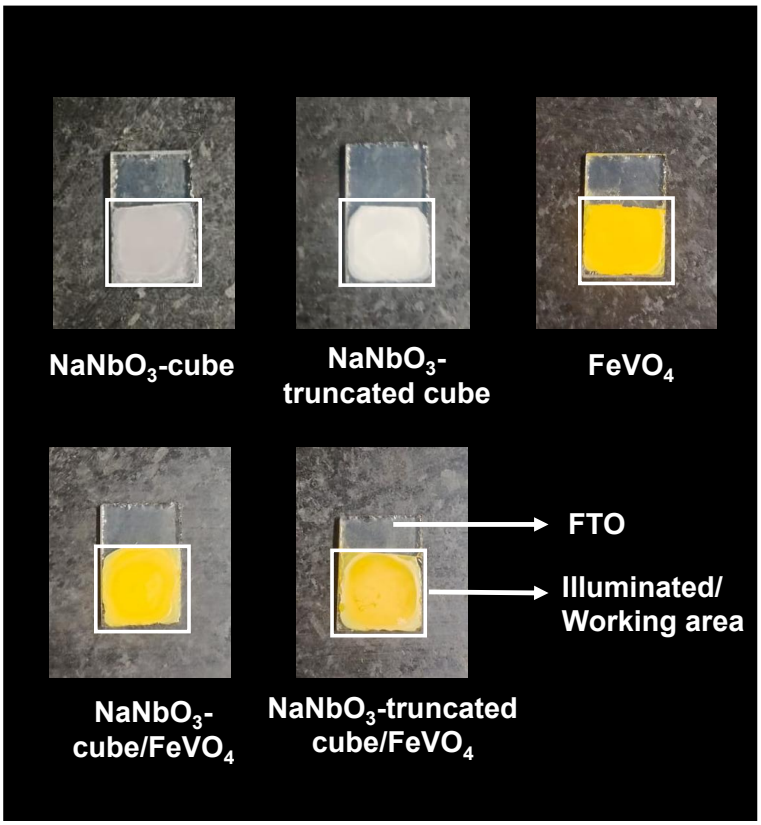

Figure S14: Digital photographs of all the electrodes.

Table S3: Comparison of current density values of the synthesized catalysts measured under dark and illuminated conditions at 1.7 V *vs.* RHE, along with ABPE values evaluated at 1.1 V *vs.* RHE.

Catalyst	$\mathbf{J}_{\text{dark}}$ (mA cm^{-2})	$\mathbf{J}_{\text{light}}$ (mA cm^{-2})	$\mathbf{J}_{\text{light}} - \mathbf{J}_{\text{dark}}$ (mA cm^{-2})	**ABPE (%)**
$NaNbO_3$-cube	0.100	0.103	0.003	1.3×10^{-4}
$NaNbO_3$-truncated cube	0.237	0.255	0.094	0.0023
$NaNbO_3$-cube/$FeVO_4$	0.227	0.377	0.140	0.0035
$NaNbO_3$-truncated cube/$FeVO_4$	0.200	0.747	0.547	0.0165

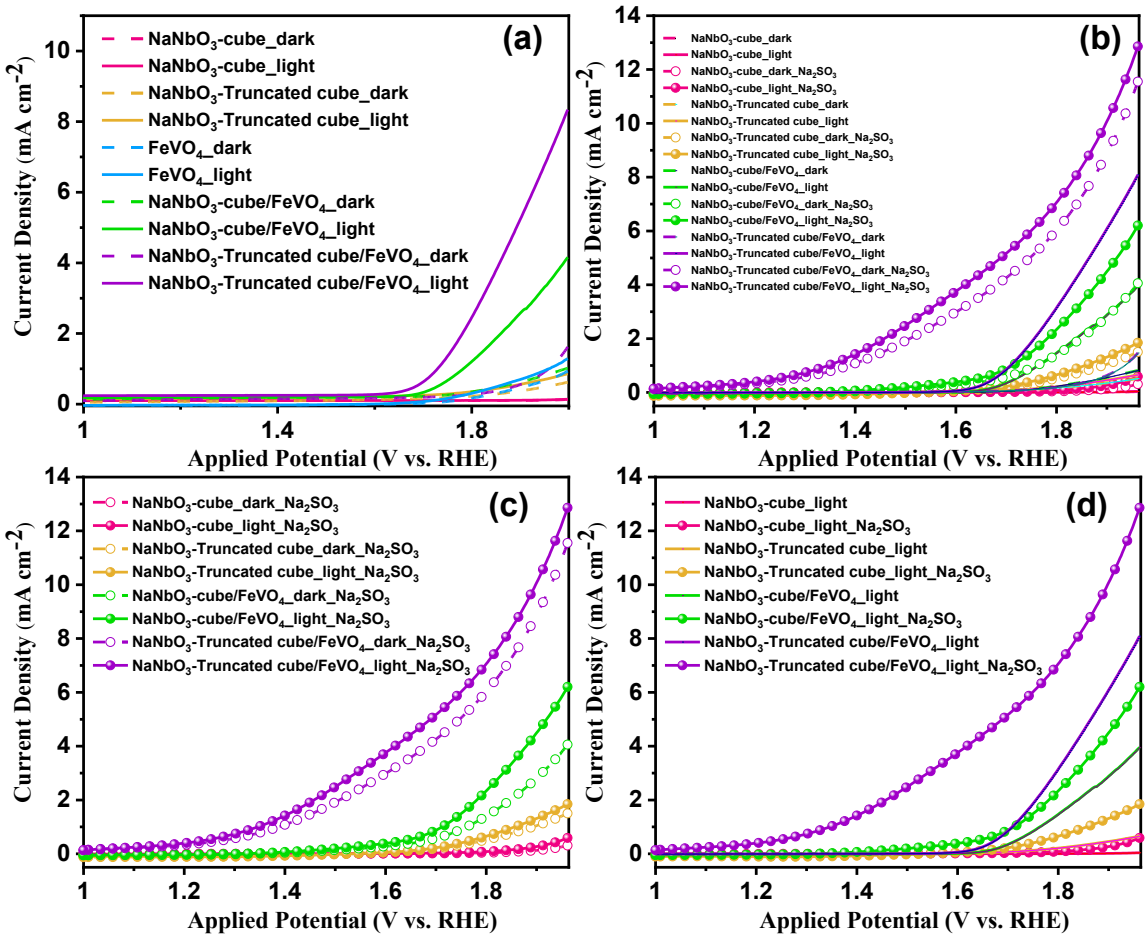

Figure S15: Polarization curves obtained from linear sweep voltammetry (LSV) measurements of the synthesized photoelectrodes recorded in the dark and under illumination. **(a)** Faceted-$NaNbO_3$, $FeVO_4$, and faceted-$NaNbO_3$/$FeVO_4$ in KOH, **(b)** faceted-$NaNbO_3$ and faceted-$NaNbO_3$/$FeVO_4$ in KOH and Na_2SO_3, **(c)** faceted-$NaNbO_3$ and faceted $NaNbO_3$/$FeVO_4$ in Na_2SO_3, and **(d)** faceted-$NaNbO_3$ and faceted-$NaNbO_3$/$FeVO_4$ in KOH and Na_2SO_3 under illumination.

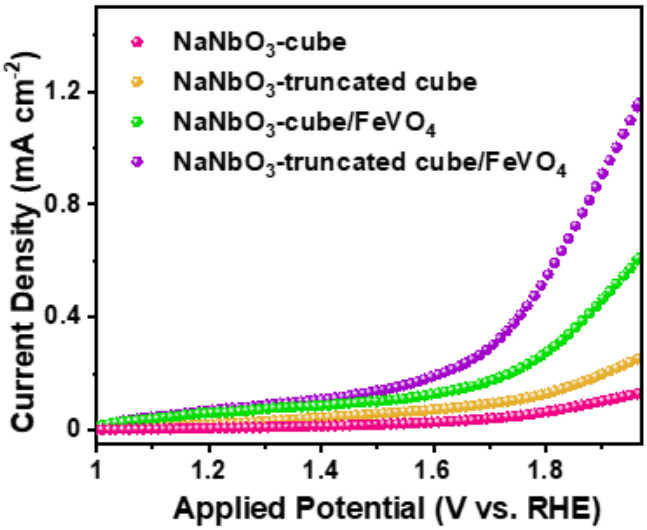

Figure S16: LSV plot of synthesized photoelectrodes in 0.5 M Na_2SO_4 under illumination.

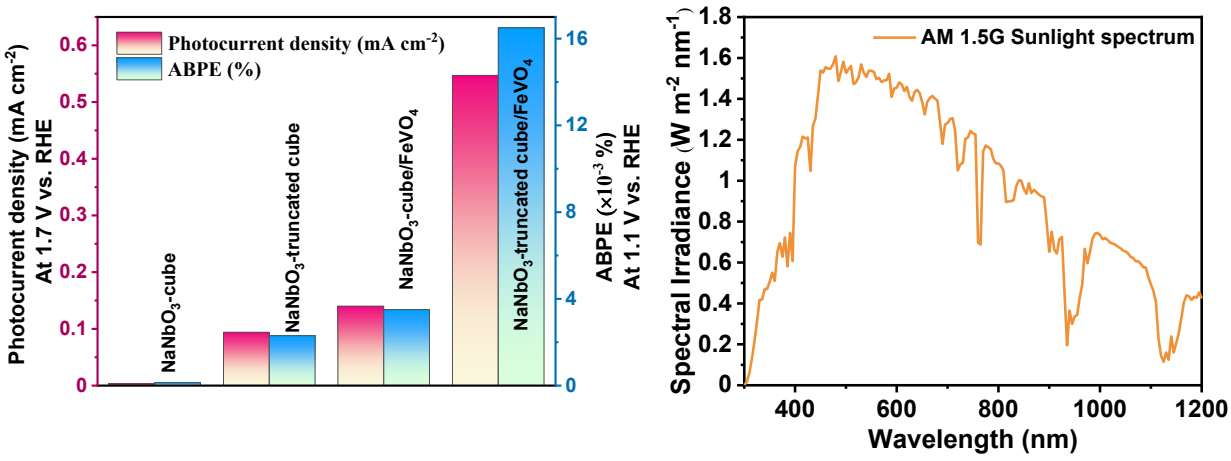

Figure S17: **(a)** Photocurrent density at 1.7 V *vs.* RHE and ABPE at 1.1 V *vs.* RHE comparison of the synthesized photoelectrodes and **(b)** light harvesting efficiency of AM 1.5 G solar simulator.

Table S4: Comparison of onset potential (V_{op}) of the synthesized catalysts measured under dark and illuminated conditions at 0.5 mA cm^{-2}.

Catalyst	$\mathbf{V}_{op,dark}$ (V *vs.* RHE)	$\mathbf{V}_{op,light}$ (V *vs.* RHE)
$NaNbO_3$-cube	1.92	1.87
$NaNbO_3$-truncated cube	1.90	1.84
$NaNbO_3$-cube/$FeVO_4$	1.85	1.72
$NaNbO_3$-truncated cube/$FeVO_4$	1.88	1.68

Table S5: Comparison of charge separation and charge transfer efficiencies of the synthesized catalysts at 1.8 V *vs.* RHE.

Catalyst	$\boldsymbol{\eta}_{separation}$ (%)	$\boldsymbol{\eta}_{transfer}$ (%)
$NaNbO_3$-cube	13.36	2.03
$NaNbO_3$-truncated cube	17.19	6.08
$NaNbO_3$-cube/$FeVO_4$	26.34	23.74
$NaNbO_3$-truncated cube/$FeVO_4$	36.76	51.69

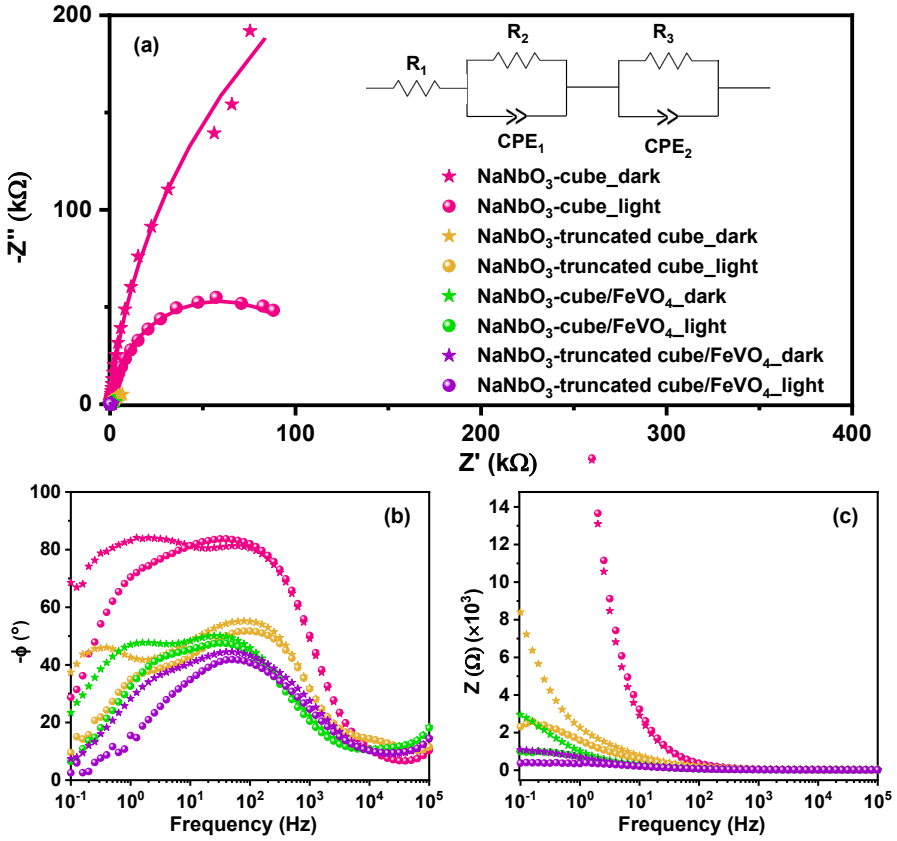

Figure S18: **(a)** Nyquist plot (inset: equivalent circuit fitted), **(b)** Bode phase, and **(c)** Bode impedance plots derived from EIS of the synthesized photoelectrocatalysts.

Table S6: EIS fitting parameters obtained for $NaNbO_3$-based photoelectrocatalysts under dark and illuminated conditions.

Synthesized Photoelectrocatalyst	$\mathbf{R_1}$ (Ω)	$\mathbf{R_2}$ (Ω)	$\mathbf{R_3}$ (Ω)
$NaNbO_3$-cube (dark)	50.96	868.53	120432.71
$NaNbO_3$-cube (light)	45.83	717.42	7106.19
$NaNbO_3$-truncated cube (dark)	49.99	865.36	14794.78
$NaNbO_3$-truncated cube (light)	28.84	700.52	3106.19
$NaNbO_3$-cube/$FeVO_4$ (dark)	20.65	385.59	3335.67
$NaNbO_3$-cube/$FeVO_4$ (light)	19.64	150.65	1102.28
$NaNbO_3$-truncated cube/$FeVO_4$ (dark)	19.94	140.72	398.59
$NaNbO_3$-truncated cube/$FeVO_4$ (light)	13.47	90.39	102.05

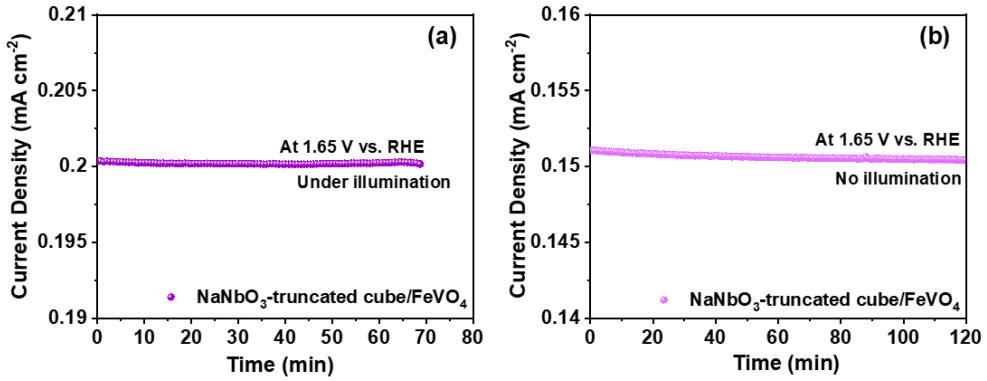

Figure S19: Long-term stability test of $NaNbO_3$-truncated cube/$FeVO_4$ at 1.65 V vs. RHE **(a)** under illumination and **(b)** no illumination.

Table S7: Characteristic peaks observed in the DRT profiles and their associated electrochemical processes.

Peak	Process	Time constant	Typical origin	Description
P1	Interfacial / ohmic contribution	$< 10^{-3}$ s	Electrode/ electrolyte interface	Represents fast processes arising from ohmic and interfacial contributions.
P2	Charge-transfer kinetics	10^{-3} to 10^{-1} s	Surface reaction sites	Corresponds to charge-transfer processes associated with electrochemical reactions.
P3	Ion-diffusion process	$> 10^{-1}$ s	Bulk electrolyte / electrode	Represents slower ion-diffusion processes within the electrode and electrolyte.

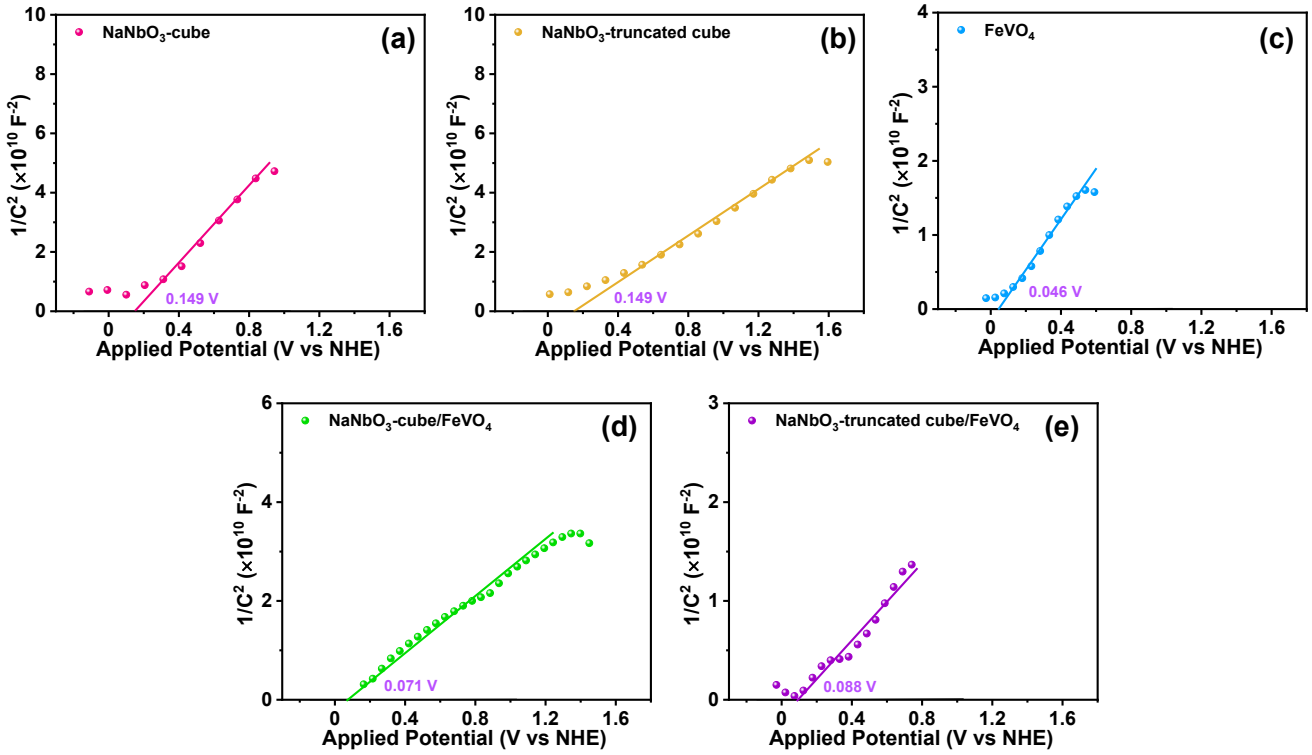

Figure S20: Mott-Schottky plots of **(a)** $NaNbO_3$-cube, **(b)** $NaNbO_3$-truncated cube, **(c)** $FeVO_4$, **(d)** $NaNbO_3$-cube/$FeVO_4$, and **(d)** $NaNbO_3$-truncated cube/$FeVO_4$.

Table S8: Charge carrier density and flat band potential values of the synthesized catalysts evaluated from Mott-Schottky plots.

Catalyst	**Charge carrier density, N_D (cm^{-3})**
$NaNbO_3$-cube	1.02×10^{19}
$NaNbO_3$-truncated cube	1.88×10^{19}
$NaNbO_3$-cube/$FeVO_4$	2.62×10^{19}
$NaNbO_3$-truncated cube/$FeVO_4$	3.54×10^{19}

Table S9: Comparative photoelectrochemical performance of the investigated photoanodes.

S. No.	Photoanode	J_{ph}	Electrolyte	Reference
1	$CdS/NaNbO_3$-nanorods	7.6 mA cm^{-2} at 0.2 V vs. SHE	0.1 M Na_2S and 0.14 M Na_2SO_3 (pH $\sim$ 12.4)	[1]
2	$NaNbO_3$@CuS	4.87 mA cm^{-2} at -0.648 V vs. Ag/AgCl	Na_2SO_4 (pH $\sim$ 7)	[2]
3	$NaNbO_3/Ag_2S$	2.44 mA cm^{-2} at 0.9 V vs. Ag/AgCl	0.5 M Na_2SO_4 (pH $\sim$ 7)	[3]
4	g-C_3N_4/$NaNbO_3$-nanofiber	12.55 mA cm^{-2} at 1 V vs. Ag/AgCl	0.5 M NaOH (pH $\sim$ 14)	[4]
5	[110]-ZnO/CdS/CdSe	4.40 mA cm^{-2} at 0 V vs. SCE	0.25 M Na_2S and 0.35 M Na_2SO_3	[5]
6	Selectively exposed TiO_2 (sTO); sTO(101), sTO(100), and sTO(001)	0.13, 0.07, and 0.02 mA cm^{-2} at 0.65 V vs. Ag/AgCl	0.5 M Na_2SO_4	[6]
7	(040) $BiVO_4$	1.26 mA cm^{-2} at 1.23 V vs. RHE	pH $\sim$ 7	[7]
8	cubic-Cu_2O and concave octahedral-Cu_2O	-0.6 mA cm^{-2} and -0.75 mA cm^{-2} at 0 V vs. RHE	0.1 M Na_2SO_4	[8]
9	(040)-$BiVO_4$	0.29 mA cm^{-2} at 1.8 V vs. RHE	0.1 M NaOH	[9]
10	{110}-$BiVO_4$, {010}-$BiVO_4$ and {110}/{010}-$BiVO_4$	0.68 mA cm^{-2}, 0.51 mA cm^{-2} and 0.31 mA cm^{-2} at 1.23 V vs. RHE	1 M KBi	[10]
11	$NaNbO_3$-cube	0.01 mA cm^{-2} at 1.9 V vs. RHE	0.1 M KOH	This work
12	$NaNbO_3$-truncated cube	0.19 mA cm^{-2} at 1.9 V vs. RHE	0.1 M KOH	This work
13	$NaNbO_3$-cube/$FeVO_4$	1.84 mA cm^{-2} at 1.9 V vs. RHE	0.1 M KOH	This work
14	$NaNbO_3$-truncated cube/$FeVO_4$	4.68 mA cm^{-2} at 1.9 V vs. RHE	0.1 M KOH	This work

References

[1] K. K. Nanda, S. Swain, B. Satpati, L. Besra and Y. S. Chaudhary, *RSC advances*, 2014, **4**, 10928–10934.

[2] S. Kumar and A. K. Ganguli, *Applied Surface Science Advances*, 2022, **9**, 100239.

[3] S. Kumar, A. P. Singh, C. Bera, M. Thirumal, B. Mehta and A. K. Ganguli, *ChemSusChem*, 2016, **9**, 1850–1858.

[4] D. Kumar, S. Sharma and N. Khare, *Nanotechnology*, 2020, **31**, 135402.

[5] J. Ma, S. Su, W. Fu, H. Yang, X. Zhou, H. Yao, Y. Chen, L. Yang, M. Sun, Y. Mu *et al.*, *CrystEngComm*, 2014, **16**, 2910–2916.

[6] C. W. Kim, S. J. Yeob, H.-M. Cheng and Y. S. Kang, *Energy & Environmental Science*, 2015, **8**, 3646–3653.

[7] L. Xia, J. Li, J. Bai, L. Li, S. Chen and B. Zhou, *Nano-Micro Letters*, 2018, **10**, 11.

[8] C. Liu, Y.-H. Chang, J. Chen and S.-P. Feng, *ACS applied materials & interfaces*, 2017, **9**, 39027–39033.

[9] Rashmi, M. D. Gyanprakash, M. Gadhewal, R. G. S. Pala and S. Sivakumar, *The Journal of Physical Chemistry C*, 2022, **126**, 16477–16491.

[10] D. Li, R. Chen, P. Wang, Z. Li, J. Zhu, F. Fan, J. Shi and C. Li, *ChemCatChem*, 2019, **11**, 3763–3769.